



Gesellschaft für Anlagen-  
und Reaktorsicherheit  
(GRS) mbH

## ADDIGAS

Advective and  
Diffuse Gas  
Transport in Rock  
Salt Formations

Final Report



**Gesellschaft für Anlagen-  
und Reaktorsicherheit  
(GRS) mbH**

## **ADDIGAS**

**Advective and  
Diffusive Gas  
Transport in Rock  
Salt Formations**

Final Report

Norbert Jockwer  
Klaus Wiczorek

April 2008

### **Remark:**

This report was prepared under the contract No. 02 E 9824 with the German Bundesministerium für Wirtschaft und Technologie (BMWi).

The work was conducted by the Gesellschaft für Anlagen- und Reaktorsicherheit (GRS) mbH.

The authors are responsible for the content of this report.

**GRS - 234  
ISBN 978-3-939355-08-3**

**Keywords:**

brine permeability, disposal of radioactive waste, EDZ, excavation disturbed zone rock salt, gas diffusivity, gas permeability, geoelectric tomography

## **Preface**

Beside granite and clay formations also rock salt is investigated as potential host rock for the disposal of radioactive waste. As a result of the mining activities the stress and strain state is changed which leads to dilatancy (i. e., volume increase, mainly caused by microfracturing) in the vicinity of the excavations. The affected area is termed as Excavation Disturbed Zone (EDZ) and is characterized by an increased porosity and permeability with micro- and potential macrofractures.

For the radioactive waste disposal in a geologic formation the properties of the EDZ with its permeability, extent, and evolution with time is of importance especially for the construction and building of geotechnical barriers. In the recent years the EDZ in rock salt formations was investigated at GRS in the frame of various projects. Main subjects of these projects were the characterisation of the EDZ with regard to its extent, hydraulic behaviour and possible healing at the in-situ stress conditions.

The main emphasis of the ADDIGAS project reported here was the evolution of the EDZ after cutting off the drift contour, the anisotropy of permeability, and the diffusive gas transport which had not been investigated in earlier projects. Moreover, an constitutive model for calculating EDZ behaviour which had been developed in the frame of the BAMBUS II project was tested.

The experimental work was performed on the 800-m level of the Asse salt mine. The project ran from 2004 to 2007 and was funded by German Ministry of Economics and Labour (BMWA) under the contract No. 02 E 9924. The modelling work was co-funded by the CEC in the frame of the Integrated Project NF-PRO under contract no. F16W-CT-2003-002389.



# Table of Contents

	<b>Preface .....</b>	<b>I</b>
<b>1</b>	<b>Introduction.....</b>	<b>1</b>
<b>2</b>	<b>Issues and Objectives .....</b>	<b>3</b>
<b>3</b>	<b>Test Field Description .....</b>	<b>5</b>
3.1	Location and Geology.....	5
3.2	Installation of the Test Field .....	6
3.3	Installations in the AHE Drift .....	12
<b>4</b>	<b>Methods of Investigation.....</b>	<b>13</b>
4.1	Gas Diffusion .....	13
4.2	Gas Permeability .....	15
4.3	Brine Injection.....	16
4.4	Geoelectric Tomography.....	18
<b>5</b>	<b>Succession of Work .....</b>	<b>21</b>
<b>6</b>	<b>Results .....</b>	<b>23</b>
6.1	Gas Diffusivity.....	23
6.2	Gas Permeability .....	28
6.3	Brine Injection and Tracking .....	31
<b>7</b>	<b>Finite Element Modelling of an Open Drift .....</b>	<b>35</b>
7.1	Geometrical Model, Constitutive laws, and Parameters .....	35
7.2	Modelling Procedure and Results .....	38

<b>8</b>	<b>Summary and Conclusions.....</b>	<b>43</b>
<b>9</b>	<b>References .....</b>	<b>47</b>
<b>10</b>	<b>List of Figures.....</b>	<b>49</b>
<b>11</b>	<b>List of Tables .....</b>	<b>51</b>

# 1 Introduction

In the repository for radioactive waste all the openings such as shafts, galleries, emplacement chambers, and disposal boreholes have to be backfilled and sealed by geotechnical barrier systems to avoid the release of radionuclides into the biosphere above an unacceptable level. The backfill and sealing materials may be crushed salt, concrete, clay, and clay-sand-mixtures, depending on the host rock and the disposal concept. In order to define the requirements for these technical barriers and to ensure long-term safety of the repository, the petrophysical and hydraulic data of the host rock in the vicinity to the artificially generated openings and in the undisturbed areas are essential.

The excavation of voids in rock salt leads to stress redistribution and displacements in the rock close to the opening. Various figures from one to five void radii have been given by different authors regarding the extent of the affected region /MLY 97/. Various expressions, like "Excavation Damaged Zone", "Disturbed Rock Zone", "Excavation Disturbed Zone", were used for the affected region. During a European Commission Cluster Conference in Luxembourg in November 2003 a clarification was achieved.

- The Excavation Damaged Zone (EDZ) in rock salt is the dilatant region close to the opening, where a volume increase (and thus porosity increase) occurs. It is characterized by microfracturing and potential macrofracturing, and the permeability of the EDZ is typically up to several orders of magnitude higher than in the undamaged rock.
- The Excavation disturbed Zone (EdZ) reaches further into the rock and covers the region where the stress field is disturbed by the excavation. Its outer limits are not as clearly defined as those of the EDZ. The EdZ outside the EDZ shows no change in hydraulic properties.

For radioactive waste disposal and particularly for the installation of geotechnical barriers knowledge of the permeability to brine and gas, the extent, and the temporal evolution of the Excavation Damaged Zone is important. Therefore, several projects aiming at the characterization of the EDZ have been performed in recent years. GRS worked on the EDZ issue in the frame of the project "Untersuchungen zur Auflockerungszone um Hohlräume im Steinsalzgebirge (ALOHA)" /WIE 98/ and the follow-up project ALOHA2 which was later integrated in "Backfill and Material Behaviour in Underground Salt Repositories, Phase II (BAMBUS II)" /BEC 04/ co-

financed by the CEC. The work focused on the characterization of the EDZ in terms of hydraulic properties and extent and on the possible self-sealing or healing of the EDZ under in-situ stress conditions. In short, the following results were obtained.

- The extent of the EDZ is less than one excavation radius.
- Close to the opening the permeability reaches values around  $10^{-15} \text{ m}^2$ . With distance from the opening it decreases continuously to the value of undamaged rock salt (around  $10^{-21} \text{ m}^2$ ).
- Permeability is highly anisotropic.
- Under favourable stress conditions EDZ permeability reduces with time ("self-sealing"), but the required time may be very long (hundreds of years).

Some of the issues, such as the anisotropy of the permeability and the dependence of EDZ properties on the time since excavation which may be important for avoiding EDZ evolution by technical means, could not be investigated to the necessary extent during the previous projects. Other information, for instance in-situ data on gas diffusion in the EDZ, was missing completely. In order to close these gaps, the ADDIGAS project was performed from 2004 to 2007.

In the frame of BAMBUS II, a model for simulating dilatancy and EDZ evolution was developed and integrated into the finite element code CODE\_BRIGTH by the Technical University of Barcelona /BEC 04/. One task of the ADDIGAS project which was performed with support of the Commission of the European Communities as a part of the Integrated Project "Understanding and physical and numerical modelling of the key-processes in the Near Field, and their coupling for different host rocks and repository strategies (NF-PRO)" under contract no. F16W-CT-2003-002389 was to use this model with the parameters identified in BAMBUS II to model the dilatancy around an open drift and compare the results to the actually measured data.

This report presents the results of ADDIGAS.

## 2 Issues and Objectives

ADDIGAS was dedicated to the issues of advective and diffusive gas transport in the EDZ that had not been resolved in the previous projects. Main emphasis was on the close vicinity to openings. A special issue was the investigation of the effectiveness of removing the EDZ, i. e., to investigate in which time and to what extent a new EDZ would evolve after cutting off the drift contour.

The specific objectives were to

- investigate permeability evolution and spatial distribution close to a drift in rock salt, especially after removing part of the EDZ,
- investigate permeability anisotropy in the EDZ, and
- investigate gas diffusion close to the drift.

For these investigations three test locations in a drift on the 800-m level of the Asse salt mine were prepared:

- one on the 20 year-old drift floor,
- a second one on the drift floor shortly after removing a one-metre layer of rock salt,
- a third one on the drift floor 2 ½ years after removal of the one-metre layer.

The test drift is located close to the so-called AHE drift where EDZ measurements were performed during the BAMBUS II. Therefore, the results from the AHE drift can be directly compared to the ADDIGAS results.

An additional objective was to calculate the EDZ evolution around an open drift using the constitutive model implemented in CODE\_BRIGHT and to check the results against the actually measured data from the AHE and ADDIGAS drifts.



### 3 Test Field Description

#### 3.1 Location and Geology

The ADDIGAS test field is located in the Asse salt mine in the north-eastern part of the anticlinal core of the salt dome (Fig. 3-1), inside the undisturbed Staßfurt Halite ( $\text{Na}_2\text{S}$ ) of the Zechstein Series which is dipping to the north-east in this part of the anticline. The Staßfurt Halite is built by a monotonous series of alternating halite ( $\text{NaCl}$ ) and sulphate layers. The thin sulphate intercalations are mainly composed of anhydrite ( $\text{CaSO}_4$ ) and polyhalite ( $\text{K}_2\text{SO}_4 \cdot \text{MgSO}_4 \cdot 2\text{CaSO}_4 \cdot 2\text{H}_2\text{O}$ ).

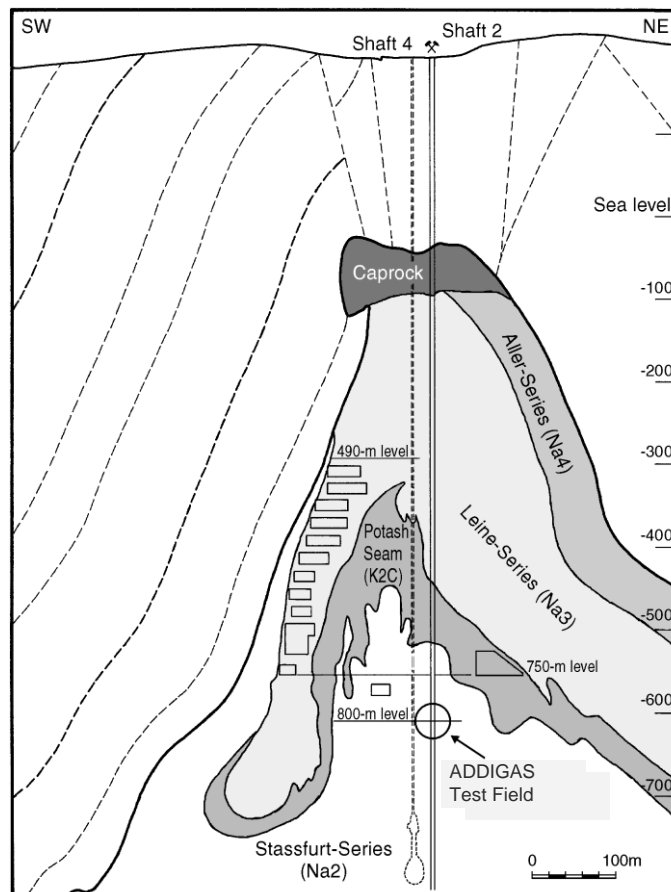


**Fig. 3-1** Cross section of the Asse salt mine with the location of the ADDIGAS test field

Between 1980 and 2000, several in-situ experiments were carried out on the 800-m level of the Asse salt mine in a part of the salt anticline which had not been significantly disturbed by former mining activities. The different test fields on the 800-m level are

shown in Fig. 3-2. The gallery in which the ADDIGAS test field was installed was excavated in 1987 and had not been used for other tests.

The AHE drift which had been used for EDZ investigations in the frame of the BAMBUS II project runs parallel to the ADDIGAS drift at a distance of approximately 20 m.

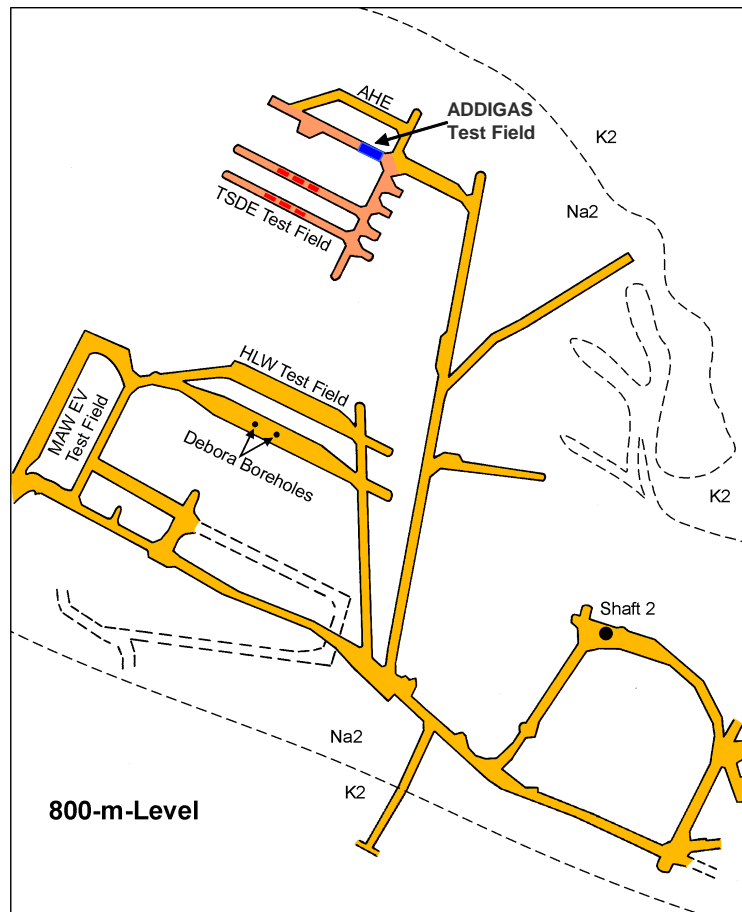


**Fig. 3-2** Plan view of the 800-m level of the Asse salt mine with the location of the ADDIGAS test field and other test areas

### 3.2 Installation of the Test Field

For the investigations of the EDZ and its evolution with time three test locations on the floor of the 20 year-old drift were prepared:

- the drift floor as existing (site B),

- the new drift floor shortly after cutting off a layer of 1 m thickness of the floor with a continuous miner (site A),
- the new drift floor about 2 ½ years after cutting off the 1-m layer (site C).

The location of the three test sites is shown in Fig. 3-3 and a photo of the test sites A and B with the 1-m cut-off and the test equipment is shown in Fig. 3-4.

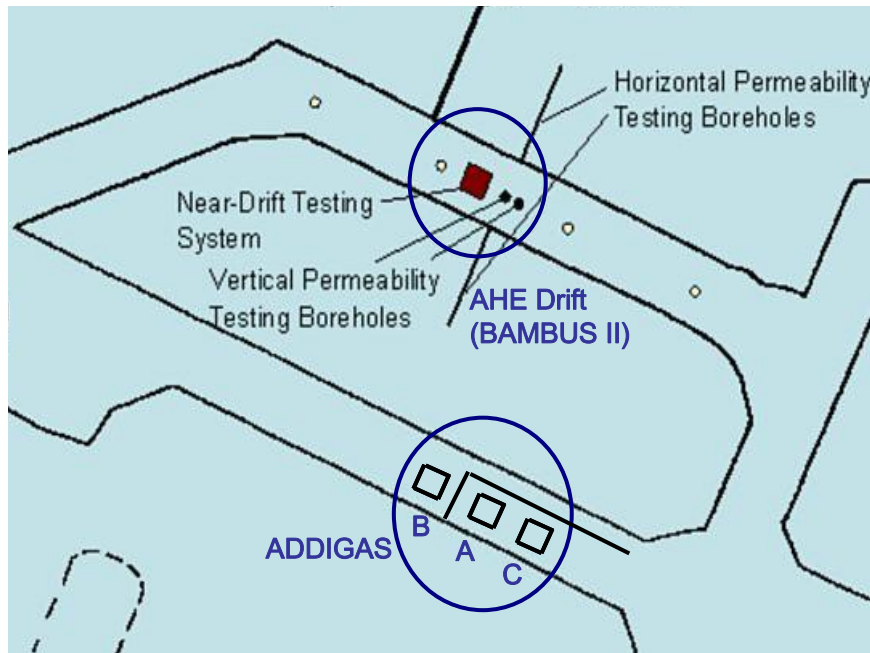


**Fig. 3-3** Plan view of the AHE drift and of the ADDIGAS test field in the 20 year-old gallery at the 800-m level of the Asse salt mine with the three test sites  
**A:** 2 months after cutting off of the EDZ  
**B:** 20 years old as existing  
**C:** 2 ½ years after cutting off the EDZ



**Fig. 3-4** Test sites A (front) and B (back) with the 1-m cut-off (site A) and the brine injection and data collection systems

Usually, in-situ measurements on gas and water permeability are performed in boreholes which are sealed with packer systems. For investigations close to the opening the boreholes and packers have to be very short and sealing to the surface is not granted. During injection tests a significant portion of the injected fluid will migrate directly through the EDZ into the drift above the borehole, so that the rock portion affected by injection may be too small for representative results. A new method was therefore developed and tested for the first time in the frame of the BAMBUS II project /BEC 04/.

A square plastic sheet with a side length of 1.8 m was embedded into a fresh layer of salt concrete and secured by screws. When the salt concrete had cured, a tight sealing of the surface to the open gallery was achieved. After installation of the sheet and curing of the salt concrete, five boreholes (BRL 1 – BRL 5) were drilled into the salt below the sheet as shown in Fig. 3-5. Each of the five boreholes is equipped with a plug at the borehole bottom which provides a 60-mm long test interval. The top of the different test intervals is 40 to 870 mm below the surface of the salt floor, respectively. The data of these boreholes at the three test sites are compiled in Tab. 3-1.

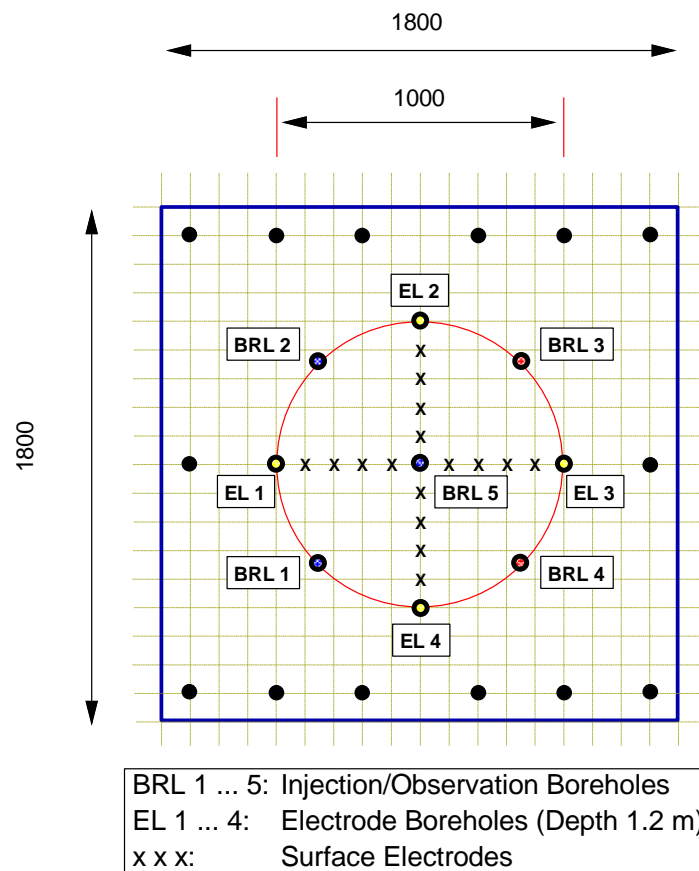


**Fig. 3-5** Plastic sheet embedded in salt concrete on the drift floor with the boreholes for injection and extraction of gas or brine (BRL 1 – BRL 5), the boreholes for the electrode chains (EL 1 – EL 4), and the surface electrodes

**Tab. 3-1** Data of the of the injection and extraction boreholes at the three test sites

Test site	Borehole BRL	Total depth [mm]	Depth in the salt [mm]	Diameter [mm]	Length of the test interval [mm]
<b>A</b>	1	150	107	25	60
	2	360	315	25	60
	3	560	515	25	60
	4	770	728	25	60
	5	155	113	25	60
<b>B</b>	1	130	100	25	60
	2	310	300	25	60
	3	535	500	25	60
	4	960	930	25	60
	5	315	300	25	60
<b>C</b>	1	160	155	25	60
	2	375	370	25	60
	3	560	555	25	60
	4	755	750	25	60
	5	175	170	25	60

Two injection/extraction tubes run from the open gallery into each interval. The borehole void above the plug is sealed with resin. At the sites A and B, four additional boreholes (EL 1 – EL 4) for installation of electrode chains were drilled and instrumented with 13 electrodes each. These boreholes were backfilled with salt concrete to ensure a good coupling of the electrodes to the rock. Additionally, 16 surface electrodes were installed in short boreholes in the salt between the electrode chains to complete the geoelectric arrays. Electrode spacing is 0.1 m.

The plastic sheet of one site with the complete arrangement of boreholes and electrodes is shown in Fig. 3-5. Fig. 3-6 shows a cross section through a test borehole. A photograph of the borehole head with the tubes, valves and quick connectors for gas and brine injection or extraction is shown in Fig. 3-7, and Fig. 3-8 shows a photograph of the plugs installed in the boreholes.

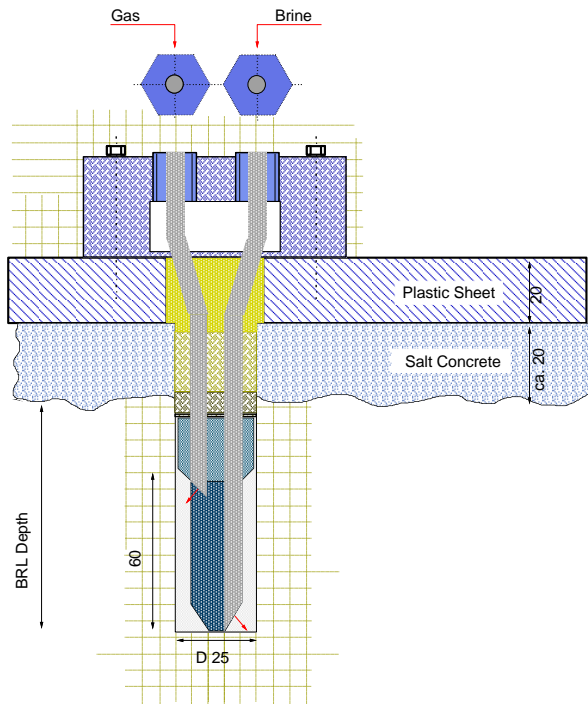


**Fig. 3-6** Cross section through a test borehole (dimensions in mm)



**Fig. 3-7** Borehole head with the tubes, valves and quick connectors for gas and brine injection or extraction



**Fig. 3-8** Plug installed in the injection and extraction boreholes

### **3.3 Installations in the AHE Drift**

The measurement system described above had been developed in the frame of BAMBUS II. The AHE drift had been equipped with one of these systems. Additionally, two horizontal boreholes in the walls and two vertical boreholes in the floor had been used for permeability testing (see Fig. 3-3) by gas injection using a four-point packer probe. The equipment is described in detail in the BAMBUS II final report /BEC 04/.

## 4 Methods of Investigation

The investigations performed comprise measurements of gas diffusivity and gas permeability as well as brine injection tests with geoelectric tracking of the brine. The methods employed are described in the following sections.

### 4.1 Gas Diffusion

Gas migration in porous media depends on the petrophysical parameters porosity, diffusivity, and permeability, but also on the solution of the gases in the aqueous phase and on the physico-chemical interaction of the gases with the internal surfaces of the different media. The solubility to water might also be of importance as rock salt contains up to 0.1 weight% of water adsorbed to the internal surfaces or trapped in fluid inclusions. In order to determine these effects, tracer gases with different solubilities to water, different sorption behaviours, and different molecular weights as listed in Tab. 4-1 were used for the diffusion investigations. As the diffusivity in air and water is proportional to the factor  $\frac{1}{\sqrt{M}}$  /JOS 72/, this factor is also displayed in the table.

**Tab. 4-1** Tracer gases with their physical parameters relevant for gas migration

Tracer gas	Molecular weight		Diffusivity in air [m <sup>2</sup> s <sup>-1</sup> ]•10 <sup>-4</sup>	Diffusivity in water [m <sup>2</sup> s <sup>-1</sup> ]10 <sup>-9</sup>	Solubility in water (1 bar) [l gas kg <sup>-1</sup> water]
	[M]	$\frac{1}{\sqrt{M}}$			
Helium	4.0	0.50	0.698	5.8	0.0083
Neon	20.0	0.22	<i>0.307</i>	2.8	0.01
Iso-butane	56.1	0.13	<i>0.154</i>	<i>1.154</i>	0.0325
Krypton	83.8	0.11	0.149	<i>1.276</i>	0.59
Sulphur hexafluoride	146.0	0.08	0.075	<i>0.928</i>	0.0056
Nitrogen	28.0	0.19		2.34	0.0156

values are from literature /LID 94/, /DAN 92/  
*italic* values are calculated

Right after installation of a test site the residual volume of each borehole was purged and flooded at atmospheric pressure with a gas mixture of 2 vol% of helium, neon, krypton, iso-butane, and sulphur hexafluoride each (tracer gases) within the matrix of 90 vol% nitrogen. After 2 to 8 days the gas in the residual volume was extracted and the composition with regard to the tracer components was determined by a gas chromatograph. Additionally, oxygen was determined in order get information about the tightness of the system. After the first extraction the residual volume was purged and

flooded with the gas mixture again, but the second extraction and analysis was performed after 10 to 41 days. The whole procedure was repeated with a third and a fourth extraction and analysis after 50 to 169 days.

For the extraction of a representative gas sample out of the boreholes a flow board as shown in Fig. 4-1 was connected to the two valves at the head of the borehole. This flow board consists of a 100-ml syringe for taking the sample, a vacuum pump, a nitrogen bottle and a peristaltic pump. First, the internal volume of the flow board and of the syringe was evacuated and purged with nitrogen and then the system and the 100-ml syringe were flooded with nitrogen at atmospheric pressure. After opening the valves to the borehole and closing the valve of the bypass a peristaltic pump purged the system for 30 minutes in a closed circuit to receive a homogenised sample which represents the gas composition in the residual volume of the boreholes. Then the valves to the borehole and the valve of the syringe were closed before the syringe was disconnected. Its gas content was analysed by a gas chromatograph in the GRS laboratory in Braunschweig with regard to the tracer gas components and oxygen. The dilution by the nitrogen in the syringe and the capillaries of the flow board was taken into account.

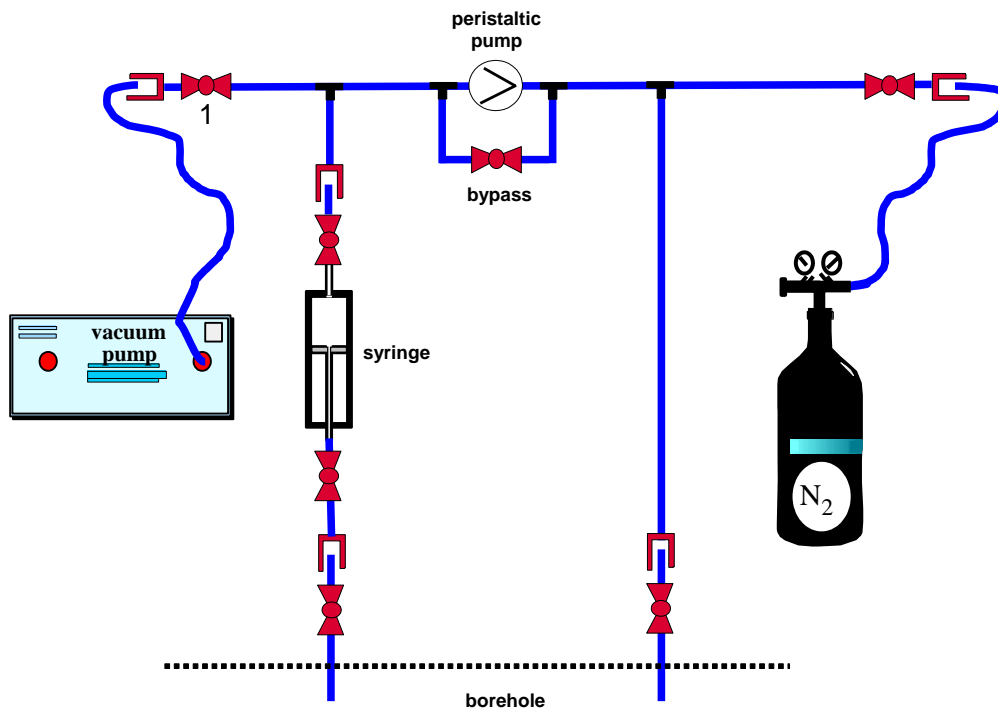


**Fig. 4-1** Flow board for extraction of gas samples out of the boreholes

With the finite element code ANSYS, taking the actual geometry around the borehole into account, the decrease of the tracer gas components versus time for the diffusion coefficients of  $10^{-8}$ ,  $10^{-9}$ , and to  $10^{-10} \text{ m}^2\text{s}^{-1}$  and borehole depths of 0.1 and 0.9 m was calculated (see Fig. 5-1 in Section 5.1). By comparison of the calculated concentrations with the ones measured the diffusion coefficient was derived.

## 4.2 Gas Permeability

Gas injection testing was performed at each of the five boreholes BRL 1 – BRL 5 of the different test sites. Nitrogen was injected at a rate of 200 ml/min up to a maximum overpressure of 1 MPa, or to a steady state if this was reached at a lower borehole pressure. The pressure evolution in all boreholes was recorded during the injection and the subsequent shut-in phase.

The gas injection system comprised a PC-based data acquisition system with pressure transducers and a programmable flow controller/flowmeter. The pressure transducers were connected to the injection/observation boreholes; each one of the boreholes could act as injection borehole by connecting a nitrogen tank via the flow controller/flowmeter. Injection rates of 20 ml/min up to 2000 ml/min and pressures up to 5 MPa were possible.

The recorded data were evaluated in terms of permeability using the computer code WELTEST 200. It provides means to calculate the analytic solution to the diffusion equation or to numerically model pressure distribution in one- or two-dimensional models, and to iteratively minimize the deviation between the measured and calculated pressure data. For measurements with gas, the real pressure has to be transformed into the so-called pseudo-pressure  $m(p)$  due to the highly pressure-dependent material properties of gas:

$$m(p) = 2 \int_{p_i}^p \frac{p}{\mu(p)z(p)} dp$$

with the initial pressure  $p_i$ , the viscosity  $\mu(p)$ , and the  $z$ -factor  $z(p)$ .

The parameters affecting the calculated pressure evolution are the rock permeability, the rock porosity, the wellbore storage coefficient, and the skin factor. The skin factor

accounts for an increased or decreased permeability of a zone close to the borehole wall, which can be due to the drilling procedure. No hints to such effects have been found in the relatively small test boreholes during earlier measurements; moreover, the whole rock close to the excavation is disturbed, so that no additional disturbance by drilling was regarded.

The calculated pressure curves are rather insensitive to changes in porosity. Therefore, the porosity was held constant at 0.2 %. This is a likely value for the deeper boreholes, while the porosity around the boreholes very close to the drift surface will be higher, but increasing the porosity by a factor of ten has no significant influence on the best fit permeability. Wellbore storage is important during the injection phase and controls the peak pressure reached during injection. The pressure curve form, especially during the shut-in phase, is controlled by the permeability.

For the ADDIGAS measurements the best-fit permeability was determined by one-dimensional calculation. As will be shown in Chapter 5 (and was already found in BAMBUS II), the permeability is highly anisotropic, with the component parallel to the drift much higher than the component perpendicular to the drift. Therefore, a one-dimensional model with gas flow only in radial direction from the borehole (which means parallel to the drift surface) is assumed to give better results than a two-dimensional model with isotropic permeability.

Gas injection tests were performed at different times before and after the diffusivity measurements, but prior to brine injection testing.

### **4.3 Brine Injection**

For brine injection only the central boreholes of the test sites A and B were used. During a first injection campaign saturated salt brine was injected to resaturate the pore space near the injection hole. A second injection was meant to be evaluated in terms of permeability to brine, which can be done in a similar way as the gas injection tests. The brine used for injection was a saturated IP9 solution in order to minimize chemical interaction with the rock salt.

The liquid injection system was developed and successfully used in the frame of the ALOHA project /WIE 98/. A sketch is shown in Fig. 4-2. Brine can be pumped into the test interval of the injection borehole via a filter and a flowmeter. Both the injection and

the return tube are equipped with pressure transducers. The return tube is needed to let the gas out of the test interval. The amount of brine injected is measured by the flowmeter; additionally, the brine tank is put on scales providing backup information. The pump and flowmeter are laid out for injection rates between 200 and 1800 ml/min; the maximum injection pressure is 10 MPa. A water tank can be connected instead of the brine tank in order to be able to rinse the system.

For the injection tests in the frame of ADDIGAS, however, the pump was replaced by a pressure vessel that could take 0.9 l of brine. By pressurizing the brine in the vessel by nitrogen from a gas tank, the brine was pressed into the test borehole. Maximum injection pressure was 1 MPa.

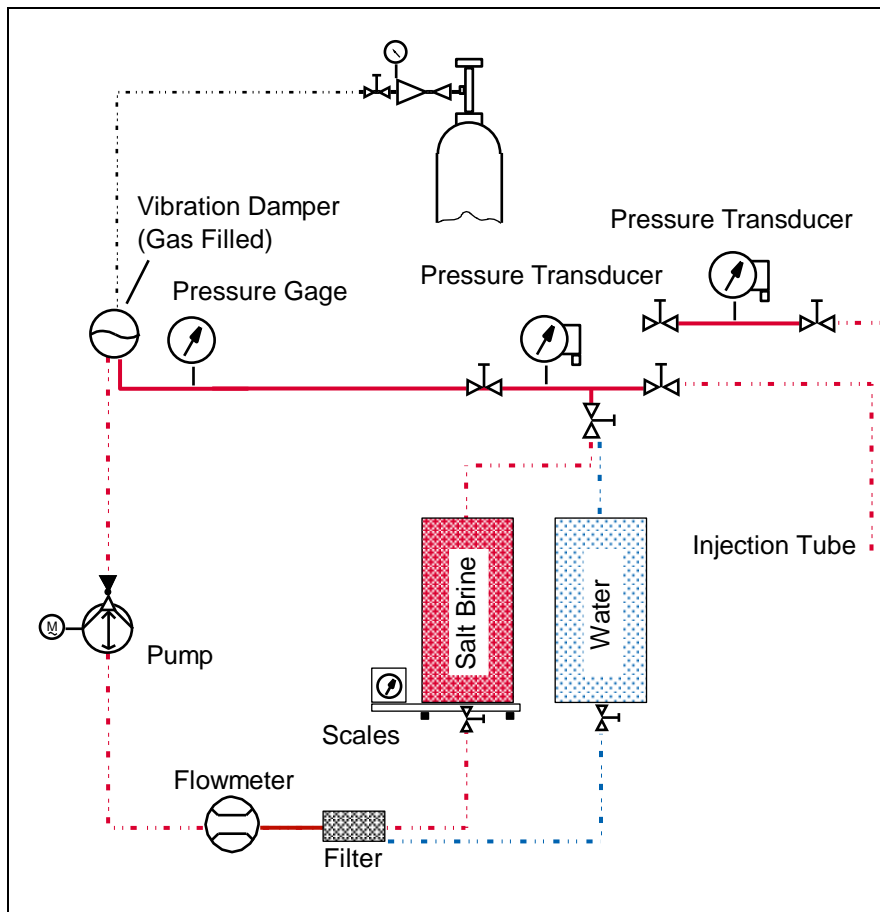


**Fig. 4-2** Liquid injection system. For ADDIGAS, the pump was replaced with a pressure vessel

#### 4.4 Geoelectric Tomography

The electric conductivity of porous rocks is determined by the pore liquid. Thus, geoelectric measurements for determination of electric resistivity and its changes are adequate for monitoring changes in the water content of such rocks. For rock salt, a broad database on the relation between resistivity and water content is available /KUL 93/ /YAR 94/ (see Fig. 4-3).

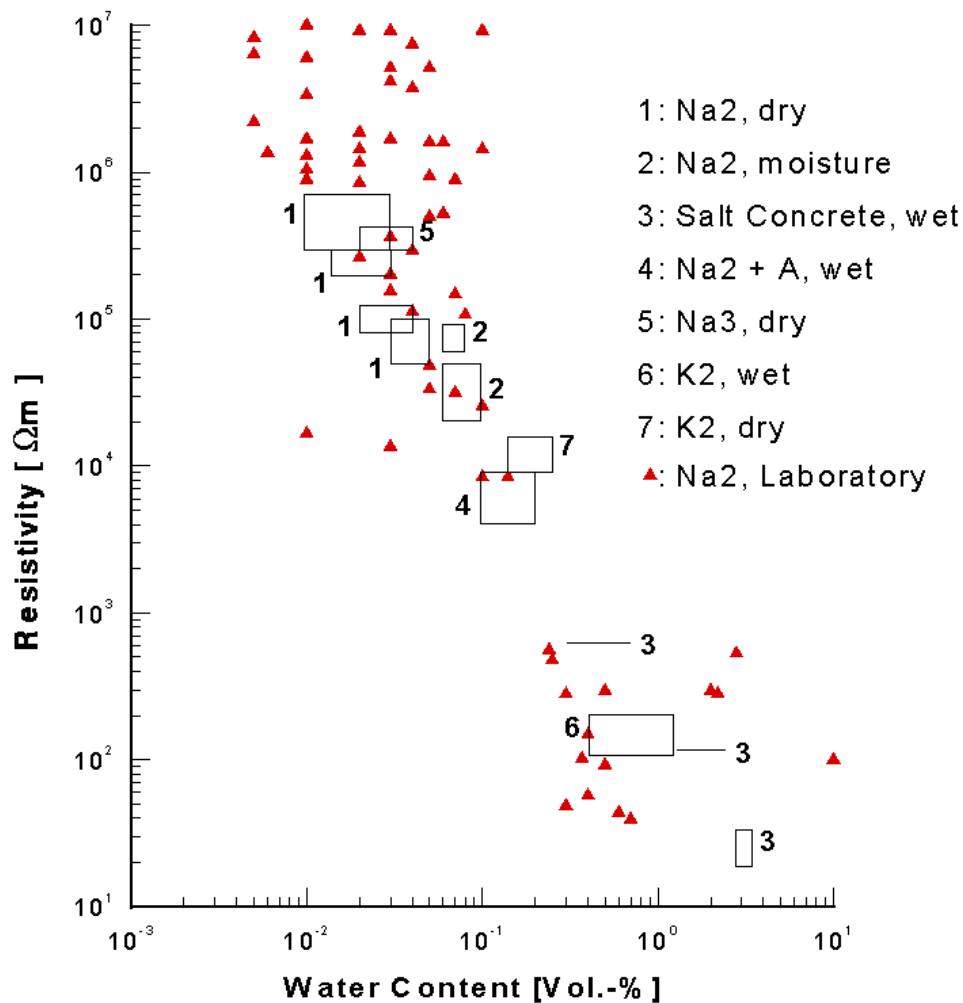


**Fig. 4-3** Relation between water content and electric resistivity for rock salt /KUL 93/ /YAR 94/

The geoelectric measurements were performed as dipole-dipole measurements: Two electrodes were used for injecting a low-frequency alternating current into the formation, while the resulting potential difference between pairs of other electrodes was measured, giving an apparent resistivity for each single measurement. The injection

and measurement dipoles were located in the same or in different boreholes and on the surface profiles. By varying both the injection dipole and the measurement dipole, a large number of single measurements was obtained.

The resulting data of the two vertical planes including the central liquid injection borehole (i.e., the plane including EL1, EL3, BRL5 and the surface electrodes in between as well as the plane including EL2, EL4, BRL5 and the corresponding surface electrodes; see Fig. 3-5) were used as input for inverse finite element modelling using the computer code SensInv2D /FEC 01/. From the vector of apparent resistivities the resistivity distribution in the considered plane was calculated as best fit between measured data and calculated response. The optimization method applied was the MSIRT (multiplicative simultaneous iterative reconstruction technique /KEM 95/).

The measuring system was an automatic geoelectric apparatus consisting essentially of the following components:

- a resistivity measuring instrument Syscal R2,
- a direct voltage source,
- a probe multiplexer with extension rack,
- a measuring and control computer.

These individual components are accommodated in a 19" rack. Up to 240 electrodes can be connected; the measurements are performed automatically. A photograph is shown in Fig. 4-4. A detailed description of the system is given by /YAR 89/. The system was successfully used in the projects ALOHA and BAMBUS II.

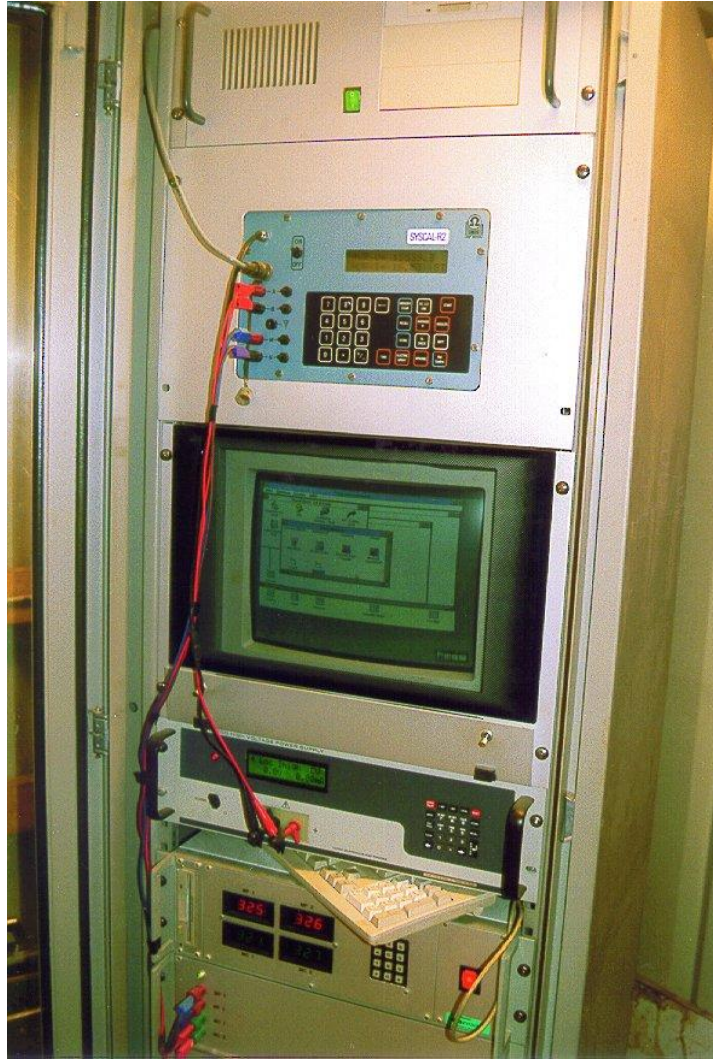


**Fig. 4-4** Geoelectric measurement system

## 5 Succession of Work

For a better overview of the different measurements and other activities, the succession of the work performed in the project is compiled in the following table.

**Tab. 5-1** Succession of work in the ADDIGAS project

<b>Time</b>	<b>Activity</b>
2004 August – September	Removal of the EDZ in part of the test drift
2004 October	Installation of the test sites A and B (plastic sheet and injection boreholes)
2004 November	Gas permeability testing, site A
2004 December – 2005 December	Diffusion testing, site A
2005 December	Gas permeability testing, site B
2006 January	Repetition of gas permeability testing, site A
2006 January – March	Diffusion testing, site B
2006 September	Installation of electrodes at test sites A and B
2007 March	Installation of test site C
2007 March – May	Diffusion testing, site C
2007 April – May	Brine injection testing, sites A and B
2007 June	Gas permeability testing, site C



## 6 Results

### 6.1 Gas Diffusivity

Measurements for determination of the gas diffusivity were performed with the components of 2 vol% helium, neon, krypton, iso-butane, and sulphur hexafluoride each in the matrix of 90 vol% nitrogen. This gas mixture was injected into the residual volume of the injection/extraction boreholes of each test site. After a time period of 2 to 169 days the gas in the residual volume was extracted for quantitative analysis with a gas chromatograph at the GRS laboratory in Braunschweig with regard to the tracer gases. The difference of the injected and extracted amount of the tracer gas component is the quota which has diffused into the surrounding host rock.

In the Tab. 6-1 to 6-3 all the results of these analyses, the concentrations of the different gas components in the boreholes of test site A, B, and C, are listed.

**Tab. 6-1** Test site A: Concentration of the different gas components as a function of time after injection in the boreholes with different depths

Borehole	Depth	Time interval	Tracer gas components				
		inject-extract	He	Ne	Kr	C <sub>4</sub> H <sub>10</sub>	SF <sub>6</sub>
	[ mm ]	[ days ]	[ vpm ]	[ vpm ]	[ vpm ]	[ vpm ]	[ vpm ]
1	107	8	4854	9441	13834	13349	14271
		48	971	3301	6505	6068	6893
		159	0	0	1286	2670	2233
		169	0	0	0	0	0
2	315	8	6294	8420	10589	9441	10164
		48	4678	9016	11737	10206	12588
		159	0	0	3360	3572	3657
		169	0	0	0	0	0
3	515	8	7310	9988	11900	11220	11603
		48	3910	7055	8500	7608	8925
		159	0	0	7863	9945	11050
		169	0	0	0	0	0
4	728	8	7126	8802	10409	9815	10130
		48	5065	8034	9431	8698	10234
		159	0	0	6846	7859	9012
		169	0	0	0	0	0
5	113	8	1016	3580	7739	8417	8659
		48	193	774	4257	5466	5611
		159	0	0	629	774	0
		169	0	0	0	0	0

**Tab. 6-2** Test site B: Concentration of the different gas components as a function of time after injection in the boreholes with different depths

Borehole	Depth	Time interval	Tracer gas components				
		inject-extract	He	Ne	Kr	C4 H10	SF6
	[ mm ]	[ days ]	[ vpm ]	[ vpm ]	[ vpm ]	[ vpm ]	[ vpm ]
1	100	7	236	0	955	812	620
		15	0	0	689	290	217
		41	0	0	729	256	222
2	300	7	261	0	1262	1741	1523
		15	1206	0	653	370	305
		41	0	0	670	283	261
3	500	7	213	0	1454	2094	1939
		15	1090	0	679	597	535
		41	0	0	586	310	295
4	930	7	715	3120	6304	7246	7701
		15	1137	747	3380	4679	5134
		41	0	0	1300	2307	2681
5	300	7	236	0	1135	1571	1222
		15	0	0	611	437	218
		41	0	0	602	249	131

In order to estimate the diffusion coefficient from the measurement results taking into account the actual geometry, a spherical finite element model of 1 m radius consisting of 682 4-node elements was developed. Diffusion was calculated for three different diffusion coefficients of the salt rock:  $D_1 = 10^{-8} \text{ m}^2/\text{s}$ ,  $D_2 = 10^{-9} \text{ m}^2/\text{s}$ , and  $D_3 = 10^{-10} \text{ m}^2/\text{s}$  over a time period of 100 days using the computer code ANSYS. Two geometries were considered: One with a borehole depth of 0.9 m, the other with a borehole depth of 0.1 m, because of the insulating effect of the plastic sheet in the case of the short boreholes. As starting concentration in the boreholes a value of 2.0 vol% (20000 vpm) was chosen for the calculation. This corresponds to the starting concentration of the tracer gas components injected into the residual volume of the boreholes. The results of this calculation are shown in Fig. 6-1.

**Tab. 6-3** Test site C: Concentration of the different gas components as a function of time after injection in the boreholes with different depths

Borehole	Depth	Time interval	Tracer gas components				
		inject-extract	He	Ne	Kr	C <sub>4</sub> H <sub>10</sub>	SF <sub>6</sub>
	[ mm ]	[ days ]	[ vpm ]	[ vpm ]	[ vpm ]	[ vpm ]	[ vpm ]
1	155	2	0	0	916	578	1784
		3	0	0	496	313	1060
		8	0	0	241	58	434
		10	0	0	145	0	159
		28	0	0	217	0	275
2	370	2	3163	6620	8012	4090	9909
		3	1455	4681	6367	2808	8476
		8	0	1012	3078	1813	4891
		10	0	308	1370	902	2361
		28	0	0	0	0	0
3	555	2	2107	4406	5633	3065	7395
		3	0	0	0	0	0
		8	38	920	2184	1073	3563
		10	0	0	0	0	0
		28	0	0	0	0	0
4	750	2	6326	9243	9278	4885	10614
		3	3866	6853	7099	2899	8716
		8	738	3585	6080	2917	8364
		10	49	1160	2390	1125	3304
		28	0	225	1560	974	2952
5	170	2	3578	2385	4962	4151	7156
		3	0	859	2863	2228	4914
		8	0	0	668	1240	1574
		10	0	0	262	573	573
		28	0	0	172	210	258

Fig. 6-2 shows the enlarged diagram for the borehole depth of 0.1 and 0.9 m, the diffusion coefficients of  $10^{-8}$ ,  $10^{-9}$  and  $10^{-10} \text{ m}^2\text{s}^{-1}$ , and the time period up to 40 days with the concentrations of the different tracer gas components determined in the residual volume of borehole BRL 2 of test site C for an example of the evaluation. This figure illustrates that the diffusion coefficients of the tracer gases are in the range between  $10^{-8}$  and  $10^{-10} \text{ m}^2\text{s}^{-1}$  and that there is a significant dependence on the molecular weight. The higher the molecular weight the lower the diffusion coefficient. But a clear dependence proportional to the factor  $\frac{1}{\sqrt{M}}$  does not exist which indicates that other effects such as sorption of the gases to the internal surfaces might influence gas diffusion in rock salt. The solubilities of the different gases in water do not influence the migration. E. g., the solubility of krypton is by a factor of 100 higher than the solubility of sulphur hexafluoride, but no corresponding relationship in the measurement results is visible. This fact is a result of the very low free water content of the rock salt.

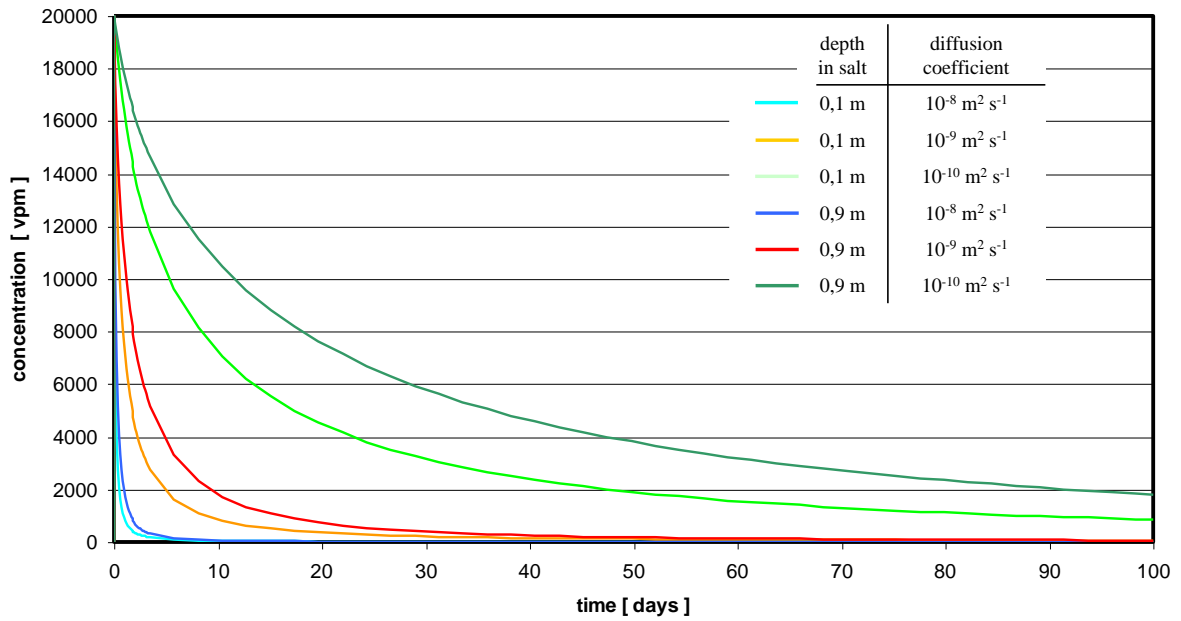


**Fig. 6-1** Decrease of tracer gas concentration versus time for different diffusion coefficients - results of the computer code ANSYS

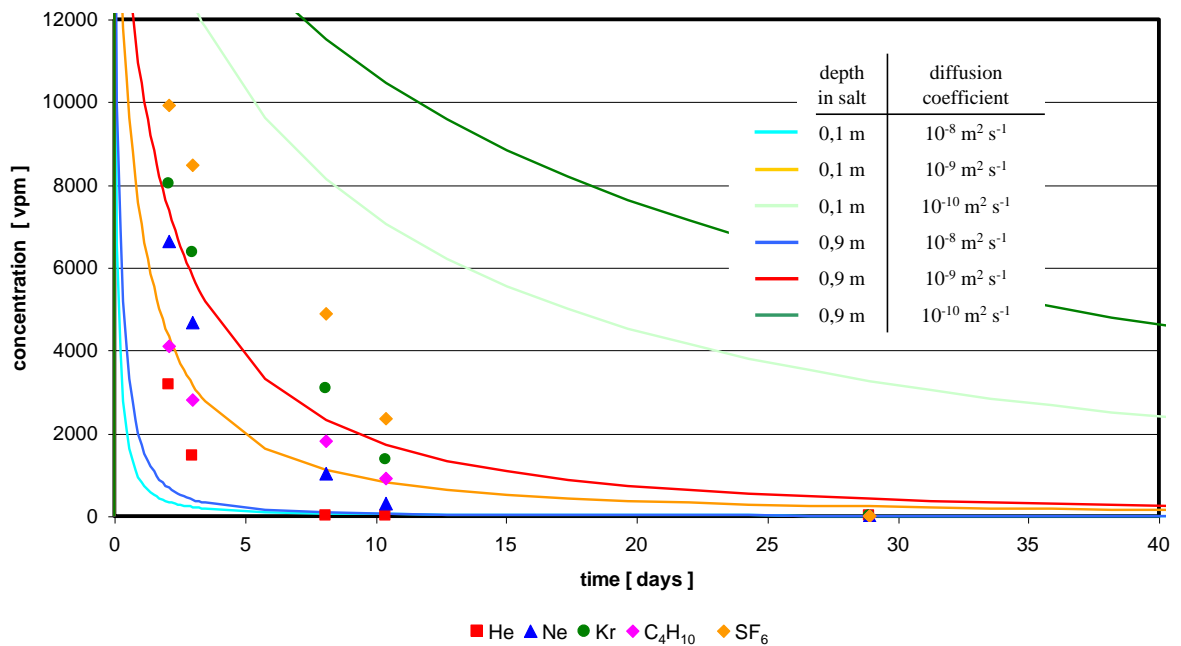


**Fig. 6-2** Enlarged section of Fig. 6-1 with the in situ results from borehole C2.  
 Lines: Results of the computer code ANSYS  
 Dots: Results of measurements test site C borehole 2

Fig. 6-3 shows the diffusion coefficients of helium in all the boreholes at all test sites. In the 20 year-old gallery floor the diffusion coefficient is close to  $10^{-8} \text{ m}^2 \text{ s}^{-1}$  down to a

depth of 0.93 m. After cutting off 1.0 m of the EDZ in the old floor, the diffusion coefficient amounts to  $10^{-9} \text{ m}^2 \text{ s}^{-1}$  at a depth of 0.1 m, decreasing to  $5 \cdot 10^{-10} \text{ m}^2 \text{ s}^{-1}$  at 0.73 m depth below the new floor eight months after EDZ removal. 2 ½ years after EDZ cut-off a new EDZ seems to be evolving. The diffusion coefficients increased to the values between  $2 \cdot 10^{-9} \text{ m}^2 \text{ s}^{-1}$  and  $8 \cdot 10^{-9} \text{ m}^2 \text{ s}^{-1}$  and, in case of test site C borehole 1, even above  $10^{-8} \text{ m}^2 \text{ s}^{-1}$ . The picture is, however, less homogeneous than for the 20 year-old EDZ.

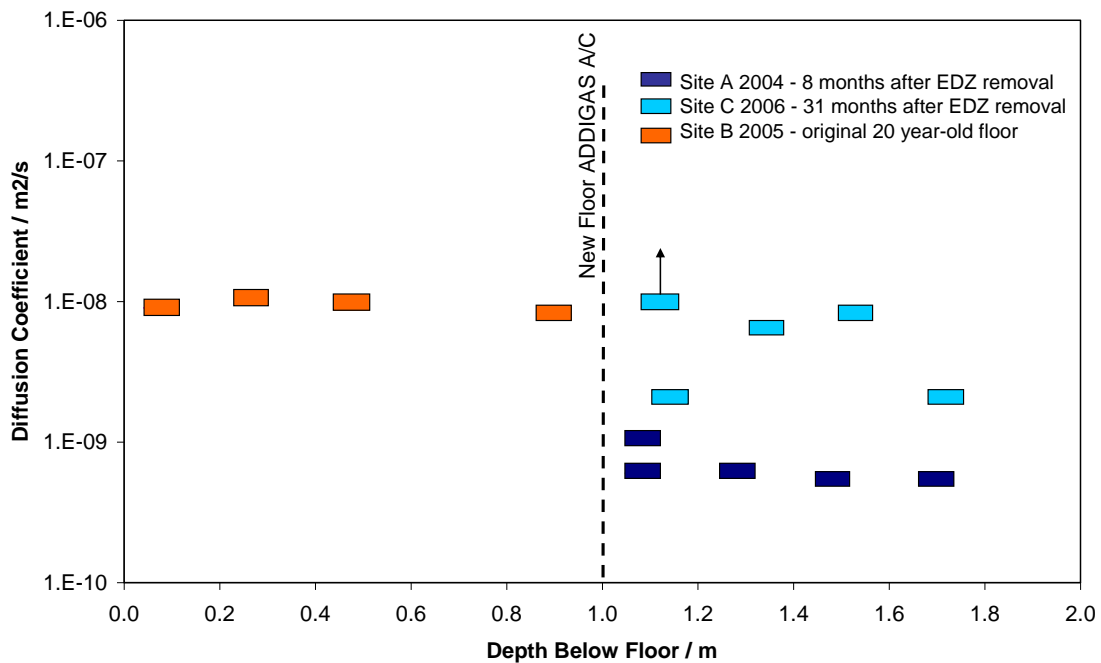


**Fig. 6-3** Diffusion coefficient of helium determined in the EDZ of the three test sites

All these results indicate:

- Significant gas diffusion can take place in rock salt even in areas where the EDZ has been cut off.
- Cutting off the EDZ temporarily reduces the diffusion by an order of magnitude.
- Gas diffusion depends on the molecular weight of the gas components - the higher the molecular weight the lower the diffusion coefficient.
- Diffusion coefficients do not depend on the solubility of the gas components to water, i. e., the low water content of rock salt (less than 0.1 weight%) prevents diffusion as dissolved gas.

## 6.2 Gas Permeability

Gas injection tests with nitrogen for the determination of permeability were performed in all test boreholes. A typical recording of the injection and the subsequent shut-in phase, transformed into pseudo-pressure (see Section 4.2) and together with the calculated best-fit curve of WELTEST, is shown in Fig. 6-4. The complete results of the permeability tests are compiled in Tab. 6-4.

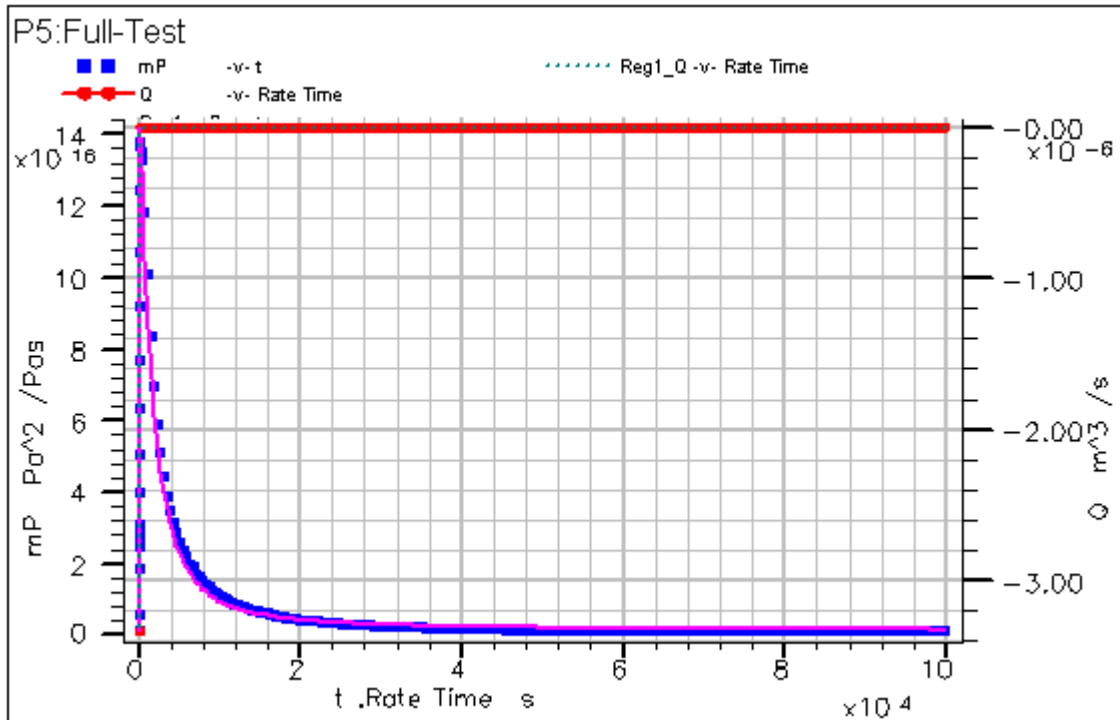


**Fig. 6-4** Pseudo-pressure and flow rate during the first gas injection test at test site A, borehole 5 (blue and red dots), together with the calculated curve for  $k = 4 \cdot 10^{-18} \text{ m}^2$  (pink)

**Tab. 6-4** Measurement results for permeability to gas

Test Site	Borehole	Depth in Salt / m	Permeability / m <sup>2</sup>
A (2 months after EDZ cut-off)	A1	0.047 – 0.107	$2.0 \cdot 10^{-18}$
	A2	0.255 – 0.315	$8.0 \cdot 10^{-20}$
	A3	0.455 – 0.515	$2.0 \cdot 10^{-20}$
	A4	0.668 – 0.728	$6.0 \cdot 10^{-21}$
	A5	0.051 – 0.113	$4.0 \cdot 10^{-18}$
A (16 months after EDZ cut-off)	A1	0.047 – 0.107	$2.0 \cdot 10^{-18}$
	A2	0.255 – 0.315	$2.0 \cdot 10^{-19}$
	A3	0.455 – 0.515	$3.0 \cdot 10^{-20}$
	A4	0.668 – 0.728	$1.5 \cdot 10^{-20}$
	A5	0.051 – 0.113	$1.5 \cdot 10^{-17}$
B (original drift floor)	B1	0.040 – 0.100	$6.5 \cdot 10^{-14}$
	B2	0.240 – 0.300	$2.4 \cdot 10^{-14}$
	B3	0.440 – 0.500	$1.6 \cdot 10^{-14}$
	B4	0.870 – 0.930	$1.5 \cdot 10^{-17}$
	B5	0.240 – 0.300	$3.7 \cdot 10^{-14}$
C (33 months after EDZ cut-off)	C1	0.095 – 0.155	$9.6 \cdot 10^{-15}$
	C2	0.310 – 0.370	$1.0 \cdot 10^{-17}$
	C3	0.495 – 0.555	$2.0 \cdot 10^{-17}$
	C4	0.690 – 0.750	$2.0 \cdot 10^{-17}$
	C5	0.110 – 0.170	$7.5 \cdot 10^{-17}$

In the 20 year-old floor at test site B permeabilities above  $10^{-14}$  m<sup>2</sup> a few centimetres below the surface were found, which decrease to about  $10^{-17}$  m<sup>2</sup> at a depth of 0.9 m. The permeability is even higher than the measurement results from the AHE drift obtained in the frame of the BAMBUS II project. During the injection tests, pressure reactions in the boreholes B2 and B3 could be seen when injecting into B5, and vice versa. B1 and B4, however, showed no reaction to injection in other boreholes, which is a clear hint to the anisotropy of permeability.

In contrast to these relatively high permeabilities found below the original floor, the measurements at the location where 1 m of salt below the floor had been removed yields permeability values of  $10^{-18}$  m<sup>2</sup> directly below the mine floor, which decreases below  $10^{-19}$  m<sup>2</sup> already at 0.3 m depth. This result agrees with earlier BAMBUS II measurements, but with packer tests performed at depths of 1 m and more below the floor.

Fig. 6-5 illustrates these results. After removal of the EDZ, namely a package of 1 m below the drift floor, the original permeability is more or less kept.

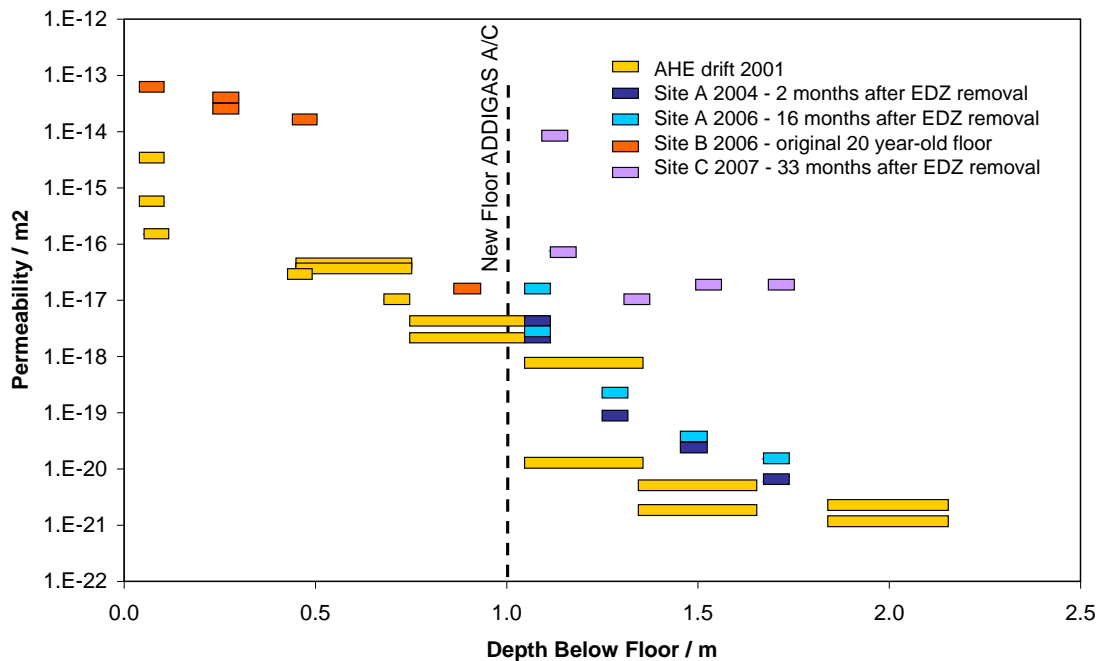


**Fig. 6-5** Permeability results obtained with the near drift testing system and packer tests below the original drift floor (AHE and ADDIGAS test site B) and below the drift floor after removal of 1 m salt (ADDIGAS test sites A and C)

The measurements at this location were performed first two months after EDZ removal. Repeating the measurements 14 months later showed only slight increases in permeability. This shows that EDZ removal is an effective method to improve seal performance.

The measurements at test site C show that a new EDZ has evolved 33 months after EDZ cut-off. With most values in the range of  $10^{-17} \text{ m}^2$  the permeability is still lower than in the old floor, but it is considerably increased compared to the undamaged rock. This result is in good agreement with the diffusion tests (see Section 6.1). Again, borehole 1 of test site C shows a particularly high value of nearly  $10^{-14} \text{ m}^2$ .

### 6.3 Brine Injection and Tracking

A liquid injection test performed in the frame of BAMBUS II /BEC 04/ had shown that all the brine (in total 8.8 l) injected into the central borehole of 10 cm depth remained in the upper 30 cm layer below the floor. This is illustrated by the Fig. 6-6 which shows the resistivity distribution in the rock before and after the brine injection: The geoelectric measurement performed prior to brine injection, Figure shows a very smooth tomogram with resistivities of 10000 to 60000  $\Omega\text{m}$  and higher resistivities towards the sides and the lower border of the investigation area as effects of the model borders. The values are in the range of typical rock salt. After the brine injection a pronounced decrease of resistivity can be detected, but it is restricted to the uppermost 30 cm below the floor.

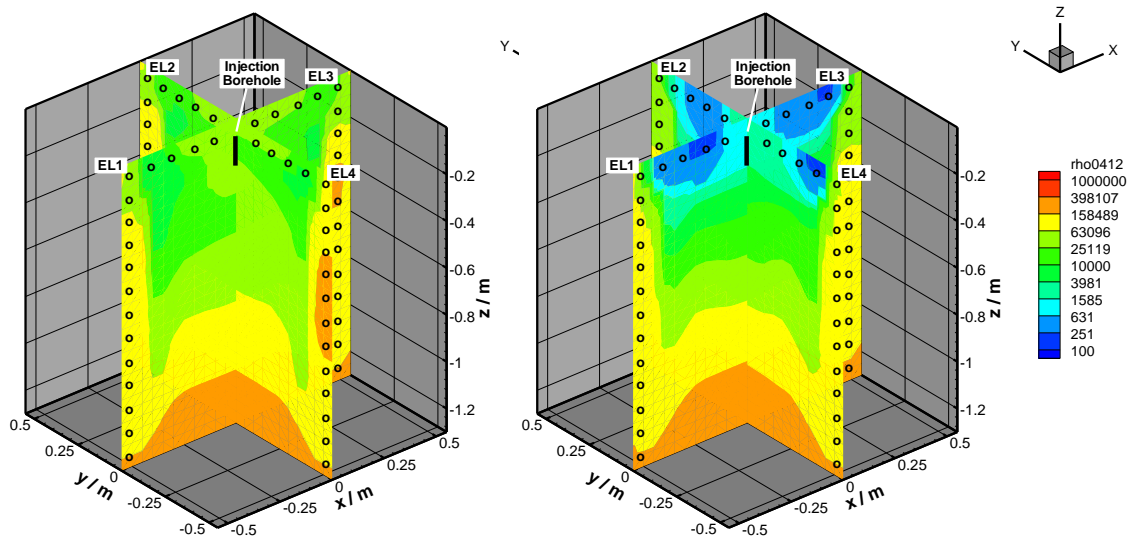


**Fig. 6-6** Resistivity tomograms of the near-surface testing arrangement obtained before (left) and after (right) a brine injection campaign in the frame of BAMBUS II (scale in  $\Omega\text{m}$ )

The resistivity of the moist zone ranged down to 200  $\Omega\text{m}$  which corresponds to a water content around 1 vol%. Assuming a radial spread of the brine in a layer of 30 cm and a uniform water content of 1 vol%, the radius of the moist zone would be 1 m, which is, again, in good agreement with observations during injection (the side length of the sheet is 1.8 m, and the first centimetres of salt beyond the sheet became wet).

Since only partial saturation was reached during the brine injection test, the porosity of the uppermost decimetres of the salt has to be considerably higher than 1 %.

In the frame of ADDIGAS, brine injection campaigns had been planned for the test sites A and B. At test site A, however, no brine injection was possible at pressures up to 1 MPa. At this overpressure the connection between borehole plug and plastic sheet became untight. Therefore, the injection test had to be stopped.

The brine staying close to the surface during the injection tests in the frame of BAMBUS II are not a clear proof for the permeability component parallel to the drift surface being higher than the perpendicular component, since permeability is decreasing with depth. Therefore, the central test interval at site B of ADDIGAS was placed at a depth between 0.24 and 03 m – in the EDZ, but not directly at the surface. 1.4 l of brine was injected into borehole 5 of test site B on May 2, 2007. On May 8, another 1.3 l was injected. Similar to the observations in BAMBUS II, the permeability to brine could not be derived from the pressure curves, because pressure fell immediately with the end of injection.

The geoelectric resistivity tomograms taken before the first injection, shortly after the first injection, directly before the second injection and after the second injection are shown in Fig. 6-7. Again, the resistivity measured before the first injection phase is typically high. Then, after the first brine injection, resistivity decreases to values between 1000 and 5000  $\Omega\text{m}$  only in the injection depth, which corresponds to a water content around 0.1 vol% (see Fig. 4.3). During the following days, the brine migrated also upward (see blue region near EL4 in the lower left picture of Fig. 6-7). During the second brine injection the low resistivity region is enlarged.

These results show that the brine tends to remain at the injection depth. Only with time it distributes to the regions above and below the injection depth. This is again a clear hint to permeability anisotropy and agrees well with the results of gas permeability testing (see Section 6.2). In particular, the anisotropy is not only due to the permeability decreasing with depth, but clearly the component parallel to the drift surface of the permeability is significantly higher than the perpendicular component. This can be expected if the microfractures causing the permeability increase are oriented parallel to the drift surface. From the stress field around the opening and from laboratory testing this is likely, and it is confirmed by the in-situ measurement results

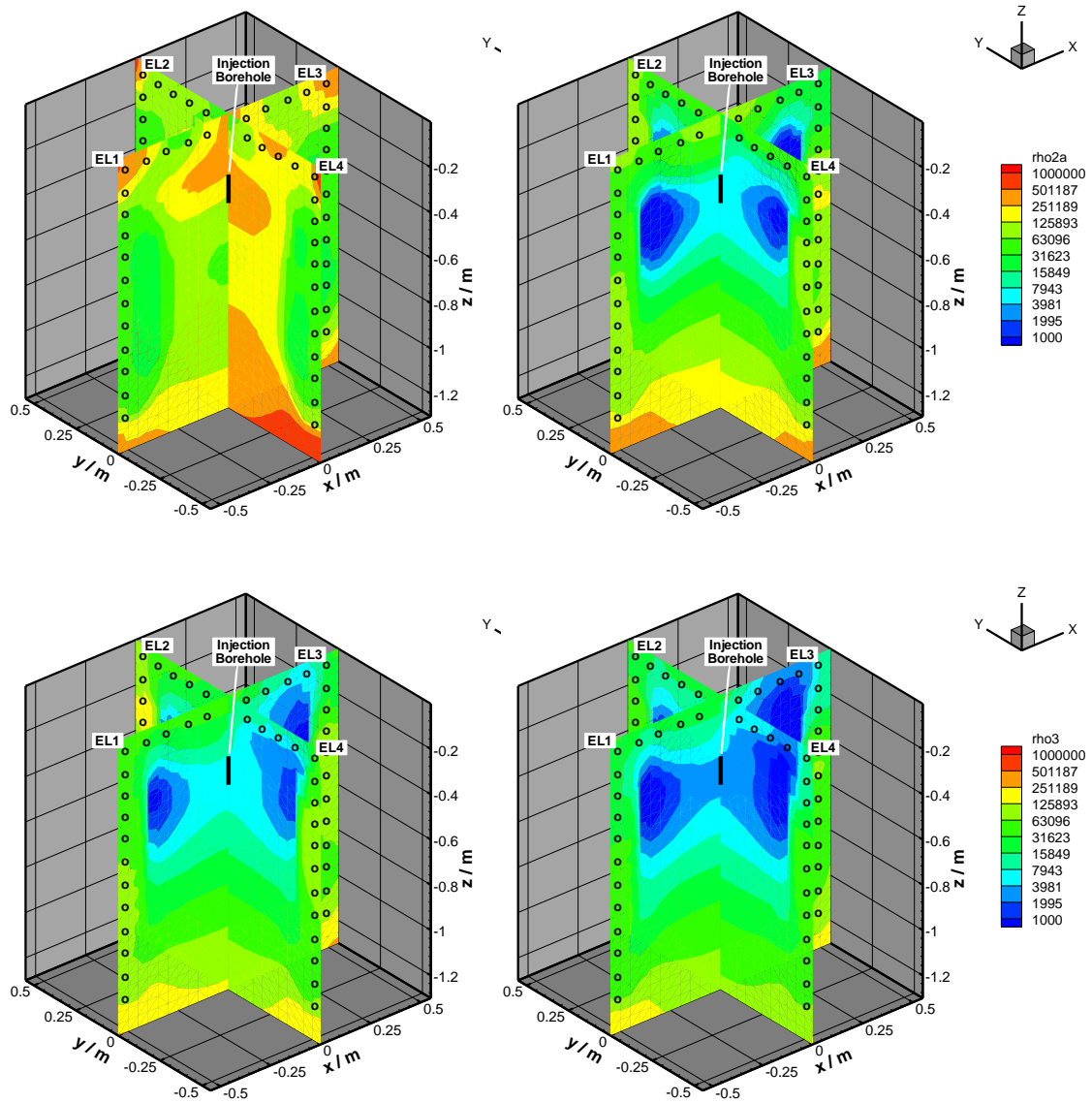


**Fig. 6-7** Resistivity tomograms of the near-surface testing arrangement obtained at test site B before (upper left) and after (upper right) the first brine injection and before (lower left) and after (lower right) the second brine injection (scale in  $\Omega\text{m}$ )



## **7 Finite Element Modelling of an Open Drift**

The objective of the modelling work performed in the frame of NF-PRO WP4.4 was to use the material models implemented in CODE\_BRIGHT /UPC 02/ with the parameters identified in BAMBUS II to simulate an open drift in rock salt and compare the results to the measurement results obtained in the AHE drift and the ADDIGAS test field to find out whether EDZ evolution in salt can be modelled with existing means or what calibration work is necessary.

This chapter presents the calculation model and the employed constitutive laws and parameters as well as the calculation results.

### **7.1 Geometrical Model, Constitutive laws, and Parameters**

The numerical simulation of the drift was performed using a rectangular plane strain model of 621 quadratic elements with 661 nodes and dimensions of 100 m by 200 m (see Fig. 7-1). The bottom line of the model was fixed in vertical direction, the left side in horizontal direction (symmetry line through the drift centre). The drift has a cross section of 4.5 m by 4 m.

In 1996, overcoring tests in the north wall of the AHE drift performed by the Bundesanstalt für Geowissenschaften und Rohstoffe (BGR) yielded stress values of 12.5 MPa in the region undisturbed by the excavation /HEU 96/. Therefore, a uniform pressure of 12.5 MPa was applied as boundary condition from the top and the right hand side of the model. Gravity was neglected. A uniform temperature of 35 °C was assumed. The initial porosity was set to 0.1%.

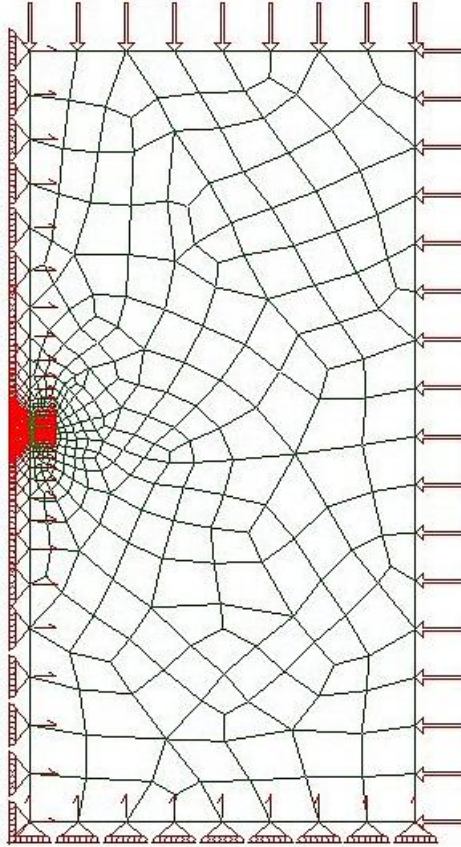


**Fig. 7-1** Finite element mesh used for the open drift simulation

Rock salt was modelled using the following constitutive laws:

- Linear elasticity
- Dislocation creep

$$\frac{d_{\varepsilon}^{DC}}{dt} = \frac{1}{\eta_{DC}^d} \Phi(F) \frac{\partial G}{\partial \sigma'}$$

with the effective stress  $\sigma'$ .

Flow rule G and stress function F:

$$F = G = \sqrt{q^2 + \left(\frac{-p}{\alpha_p}\right)^2}$$

with the stress invariants p and q.

Scalar function:

$$\Phi(F) = F^n$$

with the power n from the rock power law.

$$a_p = \left( \frac{\eta_{DC}^v}{\eta_{DC}^d} \right)^{\frac{1}{\eta+1}} \text{ with the volumetric and deviatoric viscosities}$$

$$\frac{1}{\eta_{DC}^v} = A(T) g_{DC}^v(e) \quad \text{with} \quad \frac{1}{\eta_{DC}^d} = A(T) g_{DC}^d(e) \quad \text{where } e = \text{void ratio and}$$

$$A(T) = A_A \exp\left(-\frac{Q_A}{RT}\right)$$

$$g_{DC}^v(e) = 3(G-1)^n f$$

$$g_{DC}^d(e) = \left( \sqrt{\frac{1+g+g^2}{3}} \right)^{\eta-1} \left( \frac{2g+1}{3} \right) f + \frac{1}{\sqrt{g}}$$

with

$$f = \sqrt{\frac{2e}{3(1-e^{3/2})(1+e)}} \quad \text{and} \quad g = \frac{1}{(1-f)^2}$$

- Viscoplastic deformation

$$\frac{d\varepsilon^{VP}}{dt} = \frac{1}{\eta_{VP}^d} \left\langle \Phi(F^{VP}) \right\rangle \frac{\partial F^{VP}}{\partial \sigma'} \quad \text{with} \quad \Phi(F^{VP}) = (F^{VP})^n \quad \text{and} \quad F^{VP} = \sqrt{q^2 + M^2(p - p_0)}$$

with the history variable  $p_0 = a(\varepsilon_v^{inelastic})^m$  for the inelastic volumetric deformation.

- Porosity/permeability coupling

$$k = k_0 \left( \frac{\phi}{\phi_0} \right)^m \quad \text{or} \quad k = k_0 \frac{\phi^3}{(1-\phi)^2} \frac{(1-\phi_0)^2}{\phi_0^3}$$

Although there is a volumetric part in the equation for dislocation creep, it can only account for compaction, but not for dilatancy. Therefore, another viscoplastic term had been introduced and implemented in CODE\_BRIGHT by Olivella in the frame of BAMBUS II. The parameters had been identified from the TSDE test /BEC 04/. The same materials parameters were used for the drift simulation. They are summarized in Tab. 7-1. While the parameters for elastic and creep deformation are well established, it was understood that the viscoplastic law and parameters were very provisional. The idea of the simulation with this material law was to find out whether it describes the dilatancy behaviour of rock salt in principle.

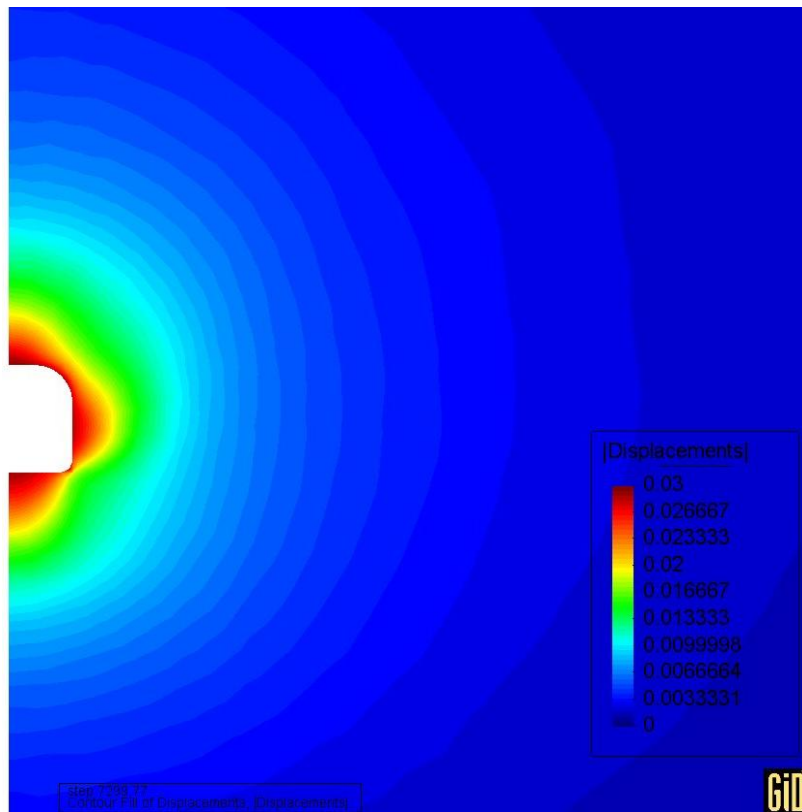
**Tab. 7-1** Material parameters for the drift simulation

Parameter	Dimension	Value
ELASTIC DEFORMATION		
Young's modulus	MPa	25000
Poisson's ratio	-	0.27
DISLOCATION CREEP		
Pre-exp. Parameter $A_A$	-	2.08e-06
Activation energy $Q_A$	J/mol	54000
Stress exponent $n$	-	5
VISCOPLASTIC DEFORM.		
Fluidity parameter $\eta_{VP}^d$	1/s	0.005
Activation energy $Q_A$	J/mol	54000
$n$ power term	-	3
$m$ power term	-	4
$a$ coefficient	-	3400
$P_0$	MPa	15

## 7.2 Modelling Procedure and Results

With the geometrical model, the boundary conditions, and the material laws and parameters presented in the previous section, a simulation calculation with CODE\_BRIGHT was performed. At first, a homogeneous model without excavation was allowed to equilibrate under the boundary stress for 10 days calculation time. Then, the elements representing the drift were removed to simulate excavation. Afterwards, simulation was continued with the open drift for a calculation time of 20 years.

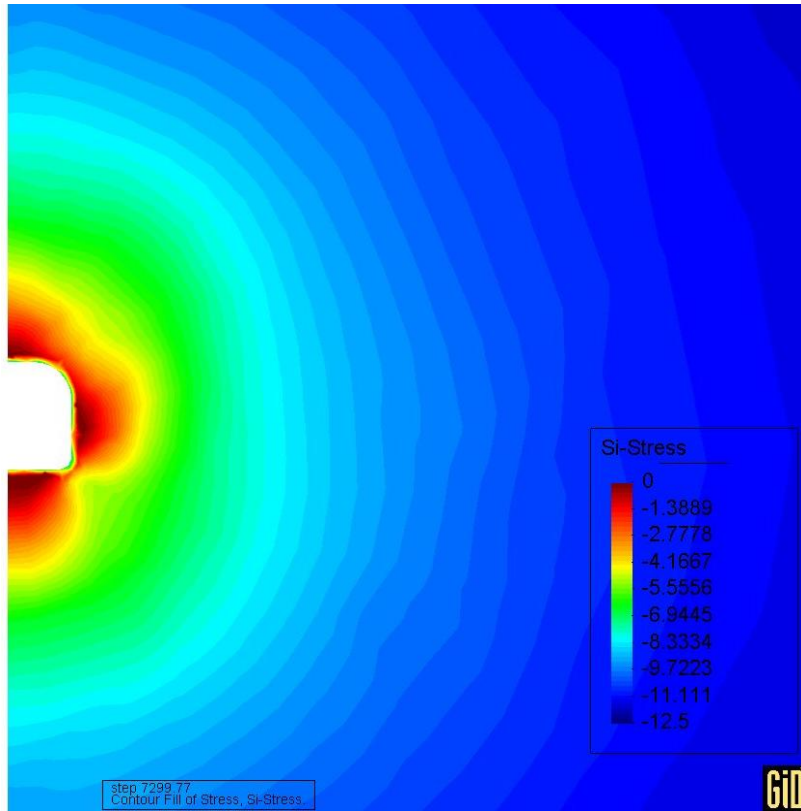
The total displacements near the drift at the end of the calculation period are shown in Fig. 7-2. As expected, the largest displacements of about 3 cm occur in the roof and the floor of the drift, the horizontal convergence is a little lower.



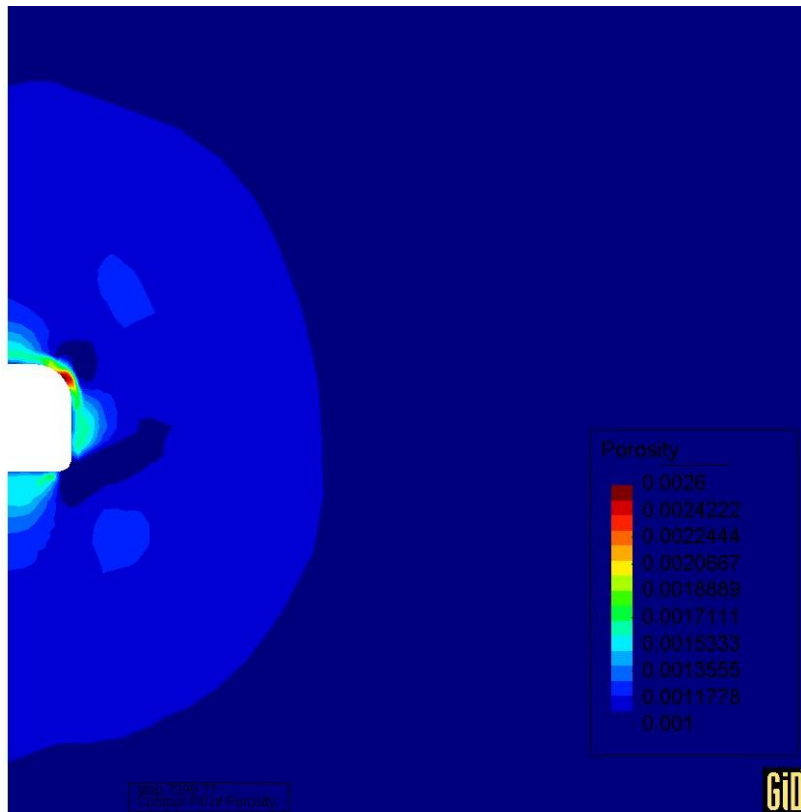
**Fig. 7-2** Total displacements near the open drift after 20 years

Fig. 7-3 shows the minimum principal stress at the end of the calculation period. The region of drastically decreased stress which is characteristic for the EDZ extends furthest into the floor, but also in the roof and the walls there are significant areas of low principal stress. Stress and deformation show a coherent picture.

The resulting porosity is shown in Fig. 7-4. The light-blue area of increased porosity around the drift covers more or less the region that would, after the results of the permeability measurements in the AHE drift and the ADDIGAS test field (see Section 6.2), be expected to show an effect. In that sense the constitutive model seems to be adequate for EDZ modelling. The porosity increase, however, is too low, at least below the drift floor. While the brine injection tests in the AHE drift (see Section 6.3) gave clear hints to porosities above 1%, only values around 0.15% are reached in the simulation. The highest porosity, about 0.25%, is reached where drift roof and wall meet. The reason for this is unclear.



**Fig. 7-3** Minimum principal stress near the open drift after 20 years



**Fig. 7-4** Calculated porosity near the open drift after 20 years

It has to be stated again that it could not be expected to reach a perfect match of the in-situ results with the provisional parameters used in this simulation. It is, on the other hand, important that a consistent set of calculation results which describes the behaviour in principle correctly has been achieved.

Since the simulated porosities are far from the expected in-situ values, it was not considered useful to look into a simulation of permeability, since in CODE\_BRIGHT permeability is calculated via a porosity/permeability relation. This would have made sense only if realistic porosity values had been calculated.

In order to achieve realistic modelling results on dilatancy and EDZ evolution, the constitutive laws and their parameters have to be improved. This is an objective of the project THERESA (Coupled thermal-hydrological-mechanical-chemical processes for application in repository safety assessment) co-financed by CEC under contract no. FP6-036458 which started in January 2007. Work package 3 of this project deals with coupled processes in salt host-rock repositories. Within the frame of this project UPC and GRS cooperate in the calibration of the material laws for EDZ modelling. Starting from the point presented in this document, a reliable constitutive model will be developed and applied on a large-scale reference test in the laboratory.



## 8 Summary and Conclusions

Rock salt formations of the North German salt domes are foreseen for the construction of a radioactive waste repository. After the operational phase all the openings such as shafts, galleries, chambers, and emplacement boreholes have to be backfilled and sealed by geotechnical barriers in order to avoid the release of radionuclides into the biosphere above an unacceptable limit. Materials for the technical barriers in rock salt may be crushed salt, concrete, or various clay mixtures. In order to define the requirements for these technical barriers and to ensure long-term safety of the repository, the petrophysical and hydraulic data of the host rock in the vicinity to the artificially generated openings (the Excavation Damaged Zone, EDZ) and in the undisturbed areas are essential.

In the frame of the ADDIGAS project the advective and diffusive gas transport near the opening, the evolution of a new EDZ after cutting off one metre of the drift contour, and the anisotropy of the permeability were investigated.

In a 20 year-old drift at the 800-m level of the Asse salt mine a test field was prepared and the investigations were performed on the

- 20 year-old drift floor with its EDZ as existing
- drift floor shortly after removal of the EDZ by cutting off a 1-m layer from the floor
- drift floor about 2 ½ years after EDZ removal

The methods involved were diffusion measurements by injecting tracer gases into short boreholes below plastic sheets cemented to the floor, measurements of permeability by gas injection into these boreholes, and brine injection tests with tracking of the brine spread by geoelectric tomography.

Gas migration in porous media depends on the petrophysical parameters porosity, diffusivity, and permeability, but also on the solution of the gases in the aqueous phase and on the physico-chemical interaction of the gases with the internal surfaces of the different media. In order to determine the gas diffusion, tracer gases with different solubilities to water, different sorption behaviours, and different molecular weights were used for these investigations. A tracer gas mixture of the components helium, neon, krypton, iso-butane, and sulphur-hexafluoride (2 vol% each) within a matrix of 90 vol% nitrogen was injected into the boreholes at atmospheric pressure. Afterwards the

concentration decrease versus time was determined. These results were compared with calculation results obtained with the computer code ANSYS for different diffusion coefficients to get the gas diffusion coefficients of the host rock.

In the 20 year-old gallery floor the diffusion coefficient is close to  $10^{-8} \text{ m}^2\text{s}^{-1}$  down to a depth of 0.93 m. After cutting off 1.0 m of the EDZ in the old floor, the diffusion coefficient amounts to  $10^{-9} \text{ m}^2 \text{ s}^{-1}$  at a depth of 0.1 m, decreasing to  $5 \cdot 10^{-10} \text{ m}^2\text{s}^{-1}$  at 0.73 m depth below the new floor eight months after EDZ removal. 2 ½ years after EDZ cut-off a new EDZ seems to be evolving. The diffusion coefficients increased to the values between  $2 \cdot 10^{-9} \text{ m}^2\text{s}^{-1}$  and  $8 \cdot 10^{-9} \text{ m}^2\text{s}^{-1}$ .

The results of the investigation on the diffusivity indicate that even in the almost undisturbed area significant gas diffusion takes place. By cutting off about 1 m of the EDZ the diffusion could be reduced by an order of magnitude. Furthermore, diffusion in the rock salt depends on the molecular weight of the gas components. The higher the molecular weight the lower the diffusion coefficient. Gas diffusion does not depend on the water solubility of the gas components due to the low amount of the water in rock salt. This result for rock salt is different from clay materials where the water content is comparatively high (30 weight%) /JOC 06/.

For determination of the gas permeability nitrogen injected into the boreholes with a maximum pressure of 1 MPa. The injection rate and the pressure evolution during the injection and the subsequent shut-in phase were recorded and evaluated in terms of permeability using the computer code WELTEST.

Measurements in the 20 year-old floor yielded a permeability in the range of  $10^{-14} \text{ m}^2$  close to the surface, decreasing to  $10^{-17} \text{ m}^2$  at about 1 m depth. In the new floor shortly after EDZ removal, the permeability of  $10^{-18} \text{ m}^2$  close to the floor decreased already at 30 cm depth below  $10^{-19} \text{ m}^2$ . 16 Months after EDZ removal, only a slight increase of these values was detected. About three years after EDZ cut-off, however, a significant new EDZ had evolved.

Brine injection into the EDZ below the 20 year-old floor and geoelectric tracking of the brine made the high permeability anisotropy visible. In particular, the anisotropy is not only due to the permeability decreasing with depth, but clearly the component parallel to the drift surface of the permeability is significantly higher than the perpendicular

component, which is explained by the orientation of microfractures parallel to the drift surface.

The following conclusions can be drawn from the experimental results:

- Both the permeability and the diffusivity of the salt below the floor are considerably higher if the EDZ is not removed.
- After removal of the EDZ the hydraulic properties of the salt below do not change significantly within more than a year, meaning EDZ removal is effective for improving seal performance.
- EDZ permeability is highly anisotropic, due to the orientation of microfractures.
- The employed methods of gas and brine injection and geoelectric tomography are suitable for obtaining relevant EDZ data.

Additionally to the experimental work, EDZ evolution in an open drift in rock salt was modelled using CODE\_BRIGHT with the existing material laws developed by UPC and compared to the measurement results obtained for the AHE drift in the frame of the BAMBUS II project and the ADDIGAS site B. The comparison showed that the dilatant behaviour of the EDZ can in principle be modelled using this formulation. The degree of dilatancy (i. e., the porosity increase) is, however, modelled to small. The parameters and perhaps also the formulation itself need a careful calibration. This will be done in the frame of the THERESA project in cooperation between UPC and GRS.



## 9 References

- /BEC 04/ Bechthold, W., E. Smailos, S. Heusermann, W. Bollingerfehr, B. Bazargan Sabet, T. Rothfuchs, P. Kamlot, J. Grupa, S. Olivella, F. D. Hansen (2004): Backfilling and Sealing of Underground Repositories for Radioactive Waste in Salt (BAMBUS-II Project), EUR 20621, Commission of the European Communities.
- /DAN 92/ D'Ans, Lax (1992): Taschenbuch für Chemiker und Physiker, Band 1, Physikalische Daten, Springer Verlag, Berlin.
- /FEC 01/ Fechner, T. (2001): SensInv2D-Manual, Geotomographie, Neuwied.
- /HEU 96/ Heusermann, S. (1996): Measurement of Initial Rock Stress at the Asse Salt Mine; in: The Mechanical Behavior of Salt. Proceedings of the Third Conference, Palaiseau, September 14 – 16, 1993, Trans Tech Publications.
- /JOC 06/ Jockwer, N., H. Kull, K. Wiczorek, R. Miehe, (2006): Investigation on Gas Migration, Technical Barriers Concrete and Bentonite as well as Granite of the Surrounding Host rock, Contribution to the Gas Migration Test (GMT) at the Grimsel Test Site, GRS – 221, Gesellschaft für Anlagen- und Reaktorsicherheit (GRS) mbH, ISBN 3-931995-91-7
- /JOS 72/ Jost, W., K. Haufe, (1972): Diffusion, Steinkopf Verlag, Darmstadt.
- /KEM 95/ Kemna, A. (1995): Tomographische Inversion des spezifischen Widerstandes in der Geoelektrik, Dissertation, Universität Köln.
- /KUL 93/ Kulenkampf, J., U. Yaramanci (1993). Frequency dependent complex resistivity of rock samples and related petrophysical parameters. *Geophysical prospecting* Vol. 41, p 995-1008.
- /LID 94/ Lide, D. R. (1994): CRC Handbook of Chemistry and Physics, 75th Edition, CRC Press, Boca Raton.

- /MLY 97/ Müller-Lyda, I. (1997): Erzeugung und Verbleib von Gasen in einem Endlager für radioaktive Abfälle, Bericht über den GRS-Workshop vom 29. und 30. Mai 1996 in Braunschweig, GRS-129, Gesellschaft für Anlagen- und Reaktorsicherheit (GRS) mbH.
- /UPC 02/ UPC (2002): CODE\_BRIGHT User's Guide, Departamento de Ingeniería del Terreno, E.T.S. Ingenieros de Caminos, Canales y Puertos de Barcelona, Universidad Politécnica de Cataluña.
- /WIE 98/ Wieczorek, K., U. Zimmer (1998): Untersuchungen zur Auflockerungszone um Hohlräume im Salzgebirge, Abschlussbericht, GRS-A-2651, Gesellschaft für Anlagen- und Reaktorsicherheit (GRS) mbH.
- /YAR 94/ Yaramanci, U. (1994): Relation of in situ resistivity to water content in salt rocks. *Geophysical Prospecting* Vol. 41, p 229-239.

## 10 List of Figures

Fig. 3-1	Cross section of the Asse salt mine with the location of the ADDIGAS test field .....	5
Fig. 3-2	Plan view of the 800-m level of the Asse salt mine with the location of the ADDIGAS test field and other test areas .....	6
Fig. 3-3	Plan view of the AHE drift and of the ADDIGAS test field in the 20 year-old gallery at the 800-m level of the Asse salt mine with the three test sites A: 2 months after cutting off of the EDZ B: 20 years old as existing C: 2 ½ years after cutting off the EDZ .....	7
Fig. 3-4	Test sites A (front) and B (back) with the 1-m cut-off (site A) and the brine injection and data collection systems .....	8
Fig. 3-5	Plastic sheet embedded in salt concrete on the drift floor with the boreholes for injection and extraction of gas or brine (BRL 1 – BRL 5), the boreholes for the electrode chains (EL 1 – EL 4), and the surface electrodes .....	9
Fig. 3-6	Cross section through a test borehole (dimensions in mm) .....	11
Fig. 3-7	Borehole head with the tubes, valves and quick connectors for gas and brine injection or extraction .....	11
Fig. 3-8	Plug installed in the injection and extraction boreholes .....	12
Fig. 4-1	Flow board for extraction of gas samples out of the boreholes .....	14
Fig. 4-2	Liquid injection system. For ADDIGAS, the pump was replaced with a pressure vessel .....	17
Fig. 4-3	Relation between water content and electric resistivity for rock salt /KUL 93/ /YAR 94/ .....	18
Fig. 4-4	Geoelectric measurement system .....	20
Fig. 6-1	Decrease of tracer gas concentration versus time for different diffusion coefficients - results of the computer code ANSYS .....	26
Fig. 6-2	Enlarged section of Fig. 6-1 with the in situ results from borehole C2. Lines: Results of the computer code ANSYS Dots: Results of measurements test site C borehole 2 .....	26
Fig. 6-3	Diffusion coefficient of helium determined in the EDZ of the three test sites .....	27
Fig. 6-4	Pseudo-pressure and flow rate during the first gas injection test at test site A, borehole 5 (blue and red dots), together with the calculated curve for $k = 4 \cdot 10^{-18} \text{ m}^2$ (pink) .....	28

Fig. 6-5	Permeability results obtained with the near drift testing system and packer tests below the original drift floor (AHE and ADDIGAS test site B) and below the drift floor after removal of 1 m salt (ADDIGAS test sites A and C) .....	30
Fig. 6-6	Resistivity tomograms of the near-surface testing arrangement obtained before (left) and after (right) a brine injection campaign in the frame of BAMBUS II (scale in $\Omega\text{m}$ ) .....	31
Fig. 6-7	Resistivity tomograms of the near-surface testing arrangement obtained at test site B before (upper left) and after (upper right) the first brine injection and before (lower left) and after (lower right) the second brine injection (scale in $\Omega\text{m}$ ) .....	33
Fig. 7-1	Finite element mesh used for the open drift simulation .....	36
Fig. 7-2	Total displacements near the open drift after 20 years.....	39
Fig. 7-3	Minimum principal stress near the open drift after 20 years .....	40
Fig. 7-4	Calculated porosity near the open drift after 20 years .....	40

## 11 List of Tables

Tab. 3-1	Data of the of the injection and extraction boreholes at the three test sites.....	10
Tab. 4-1	Tracer gases with their physical parameters relevant for gas migration ....	13
Tab. 5-1	Succession of work in the ADDIGAS project.....	21
Tab. 6-1	Test site A: Concentration of the different gas components as a function of time after injection in the boreholes with different depths.....	23
Tab. 6-2	Test site B: Concentration of the different gas components as a function of time after injection in the boreholes with different depths.....	24
Tab. 6-3	Test site C: Concentration of the different gas components as a function of time after injection in the boreholes with different depths.....	25
Tab. 6-4	Measurement results for permeability to gas.....	29
Tab. 7-1	Material parameters for the drift simulation .....	38

**Gesellschaft für Anlagen-  
und Reaktorsicherheit  
(GRS) mbH**

Schwertnergasse 1  
**50667 Köln**  
Telefon +49 221 2068-0  
Telefax +49 221 2068-888

Forschungsinstitute  
**85748 Garching b. München**  
Telefon +49 89 32004-0  
Telefax +49 89 32004-300

Kurfürstendamm 200  
**10719 Berlin**  
Telefon +49 30 88589-0  
Telefax +49 30 88589-111

Theodor-Heuss-Straße 4  
**38122 Braunschweig**  
Telefon +49 531 8012-0  
Telefax +49 531 8012-200

**[www.grs.de](http://www.grs.de)**